Received: 25 May 2022 | Revised: 1 October 2022 | Accepted: 18 October 2022

DOI: 10.1111/jnc.15714

Journal of Neurochemistry JNC The Official Journal of the International Society for Neurochemistry WILEY

ORIGINAL ARTICLE

Neurochemical correlates of synapse density in a Huntington's disease mouse model

Nicole Zarate[1] | Katherine Gundry[2] | Dahyun Yu[1] | Jordan Casby[3] | Lynn E. Eberly[2,4] | Gülin Öz[2] | Rocio Gomez-Pastor[1]

[1]Department of Neuroscience, Medical School, University of Minnesota, Minneapolis, Minnesota, USA

[2]Department of Radiology, Center for Magnetic Resonance Research, Medical School, University of Minnesota, Minneapolis, Minnesota, USA

[3]Department of Pharmacology, Medical School, University of Minnesota, Minneapolis, Minnesota, USA

[4]Division of Biostatistics, School of Public Health, University of Minnesota, Minneapolis, Minnesota, USA

Correspondence
Rocio Gomez-Pastor, Department of Neuroscience, Medical School, University of Minnesota, 2101 6th St. SE, Winston and Maxine Wallin Medical Biosciences Building Room 4–146 Minneapolis, MN 55455, USA.
Email: rgomezpa@umn.edu

Funding information
Institutional Center Cores for Advanced Neuroimaging, Grant/Award Number: P30 NS076408; National Institute of Biomedical Imaging and Bioengineering, Grant/Award Number: P41 EB027061; National Institute of Neurological Disorders and Stroke, Grant/Award Number: R01 NS110694; University of Minnesota, Grant/Award Number: Biomedical Research Awards for Interdisciplinary N; W. M. Keck Foundation

Abstract

Striatal medium spiny neurons are highly susceptible in Huntington's disease (HD), resulting in progressive synaptic perturbations that lead to neuronal dysfunction and death. Non-invasive imaging techniques, such as proton magnetic resonance spectroscopy (^{1}H-MRS), are used in HD mouse models and patients with HD to monitor neurochemical changes associated with neuronal health. However, the association between brain neurochemical alterations and synaptic dysregulation remains unknown, limiting our ability to monitor potential treatments that may affect synapse function. We conducted in vivo longitudinal ^{1}H-MRS in the striatum followed by ex vivo analyses of excitatory synapse density of two synaptic circuits disrupted in HD, thalamo-striatal (T-S), and cortico-striatal (C-S) pathways, to assess the relationship between neurochemical alterations and changes in synapse density. We used the zQ175$^{(Tg/0)}$ HD mouse model as well as zQ175 mice lacking one allele of CK2α'(zQ175$^{(Tg/0)}$:CK2α'$^{(+/-)}$), a kinase previously shown to regulate synapse function in HD. Longitudinal analyses of excitatory synapse density showed early and sustained reduction in T-S synapses in zQ175 mice, preceding C-S synapse depletion, which was rescued in zQ175:CK2α'$^{(+/-)}$. Changes in T-S and C-S synapses were accompanied by progressive alterations in numerous neurochemicals between WT and HD mice. Linear regression analyses showed C-S synapse number positively correlated with ^{1}H-MRS-measured levels of GABA, while T-S synapse number positively correlated with levels of phosphoethanolamine and negatively correlated with total creatine levels. These associations suggest that these neurochemical concentrations measured by ^{1}H-MRS may facilitate monitoring circuit-specific synaptic dysfunction in the zQ175 mouse model and in other HD pre-clinical studies.

KEYWORDS
^{1}H-MRS, CK2 alpha prime, Huntington's disease, neurochemicals, synapse density, zQ175

Abbreviations: CRLB, Cramér Rao Lower Bounds; C-S, cortico-striatal; CSF, cerebrospinal fluid; fMRI, function magnetic resonance imaging; GABA, gamma-aminobutyric acid; Gln, glutamine; Glu, glutamate; Gly, glycine; GSH, glutathione; HD, Huntington's disease; HTT, huntingtin; Ins, myo-inositol; Lac, lactate; MR, magnetic resonance; 1H-MRS, 1 proton magnetic resonance spectroscopy; MSN, medium spiny neuron; NAA, N-acetyl aspartate; PE, phosphoethanolamine; PET, positron emission tomography; PFA, paraformaldehyde; polyQ, poly-glutamine; ROI, region of interest; SCA, Spinocerebellar ataxia; Tau, taurine; tCho, total choline; tCr, total creatine; T-S, thalamo-striatal; VOI, volume of interest; WT, wild type.

Nicole Zarate and Katherine Gundry contributed equally to this work.

1 | INTRODUCTION

Huntington's disease (HD) is an autosomal dominant, neurodegenerative disorder caused by expansion of a trinucleotide repeat (CAG) in exon 1 of the Huntingtin gene (*HTT)* (MacDonald et al., 1993). The HTT protein is prone to protein misfolding, and its aggregation preferentially affects medium spiny neurons (MSN) of the striatum, causing synaptic perturbations and neuronal death. HD is characterized by progressive motor, cognitive, and psychiatric deficits for which there are no effective therapies. To design therapies that effectively modify disease symptoms, it is necessary to identify robust HD biomarkers able to objectively monitor cerebral pathology.

Mouse models of HD and patients with prodromal HD show perturbations in striatal synaptic stability and functional connectivity, respectively, before motor symptom onset or overt neuronal cell death (Raymond et al., 2011; Unschuld et al., 2012). MSNs receive excitatory glutamatergic input from the cortex and intralaminar nuclei of the thalamus and both D1 (direct pathway) and D2-type MSNs (indirect pathway) rely equally on these excitatory inputs (Huerta-Ocampo et al., 2014; Smith et al., 2009). Dysfunction in the cortico-striatal (C-S) pathway has been widely reported in HD, showing disruptions in this circuitry occur at symptomatic stages but prior to MSN death (Cepeda et al., 2007; Raymond et al., 2011; Unschuld et al., 2012). Recent studies in cell and mouse models of HD showed that thalamic input is also disrupted in HD and occurs before C-S circuit pathology or onset of motor symptoms (Cepeda et al., 2007; Gomez-Pastor et al., 2017; Kolodziejczyk & Raymond, 2016; Mckinstry et al., 2014), indicating that the thalamo-striatal (T-S) excitatory circuit may play a more prominent role in early HD pathogenesis.

Having the ability to monitor synaptic stability in the living brain could therefore be a powerful tool to predict disease progression as well as determine the impact of potential therapeutic strategies on synaptic function. However, in vivo monitoring of synapses in the human brain is technically challenging. Recently developed positron emission tomography (PET) radioligands targeting various synaptic vesicle proteins can be used to monitor synaptic density in both animals and humans (Finnema et al., 2016; Thomsen et al., 2021). However, the limited availability of these PET tracers and concerns about repeated radiation exposure provide motivation to assess alternative neuroimaging technologies to evaluate synapse density. Magnetic resonance (MR) methods like functional MR imaging (fMRI) and MR spectroscopy (MRS) overcome these concerns but have yet to be evaluated as markers of synaptic density.

MRS has emerged as a useful tool to evaluate neurochemical alterations in HD and other polyQ diseases (Joers et al., 2018; Öz, 2016; Öz et al., 2010; Sturrock et al., 2015). Studies in various mouse models of HD and in patients with HD have highlighted consistent alterations in key neurochemicals that can be associated with neurodegeneration, such as depletion of the neuronal integrity marker *N*-acetylaspartate (NAA) or increased levels of the putative gliosis marker *myo*-inositol (Ins) (Heikkinen et al., 2012; Peng et al., 2016; Sturrock et al., 2015; Tkác et al., 2007). However, the underpinnings of the neurochemical changes that connect them with functional decline is still unknown, limiting our understanding of how potential treatments that may affect synapse function translate into alterations of brain metabolites. Previous studies in patients with different spinocerebellar ataxias (SCAs) presenting different degrees of synapse loss proposed that neurochemical alterations measured by MRS may reflect changes in synaptic function or density (Joers et al., 2018; Öz, Iltis, et al., 2011). Consistently, a recent MRS study in aged zQ175 mice showed that key striatal neurochemical alterations paralleled changes in T-S synapses (Yu et al., 2022), highlighting the potential use of MRS as a tool to monitor synapse density. However, the relationship between neurochemical alterations and synaptic density has not been directly assessed thus far.

The use of mouse models allows for parallel characterization of neurochemical concentrations and neuropathological features, an essential aspect of understanding how different neurochemical abnormalities relate to pathology. In the present study, we conducted in vivo longitudinal high field proton (^{1}H) MRS in the striatum of the heterozygous zQ175 HD mouse model followed by ex vivo analyses of excitatory synapse densities of two major striatal synaptic circuits (C-S and T-S) differentially altered in HD. We chose for our study the heterozygous knock-in zQ175 HD mouse model (zQ175$^{Tg/0}$) for its slow disease progression and its ability to recapitulate multiple HD-like features observed in patients with HD, such as HTT aggregation, progressive synaptic deficits, transcriptional dysregulation, gliosis, weight loss, and motor and cognitive impairment (Gomez-Pastor et al., 2017; Heikkinen et al., 2012; Menalled et al., 2012). We also studied zQ175 mice lacking one allele of CK2α', a kinase involved in synapse stability in HD, the haploinsufficiency of which differentially altered T-S and C-S circuitry and ameliorated long-term HD-like symptoms (Gomez-Pastor et al., 2017; Yu et al., 2022). We found that T-S synaptic density was significantly correlated with alterations in phosphoethanolamine (PE) and total creatine (tCr) while C-S synapse number significantly correlated with gamma-aminobutyric acid (GABA). We propose that GABA, PE, and tCr alterations could be used as neurochemical markers to monitor circuit-dependent synapse dysfunction in T-S and C-S circuitries. Furthermore, these results support the possibility of using MRS as a technique in future HD pre-clinical studies to monitor treatment efficacy in altering excitatory synaptic function in the striatum.

2 | METHODS

2.1 | Mouse strains

We used a full-length heterozygous knock-in mouse model of HD known as zQ175 (#027410, RRID:IMSR_JAX:000664) on the C57BL/6J background (RRID:IMSR_JAX:000664). The knock-in heterozygous zQ175 HD mouse model was chosen because it recapitulates aspects of HD-like features, including HTT aggregation, synaptic deficits, gliosis, motor and cognitive impairments, as well as weight loss. This model also displays a slower disease progression

than other mouse models, similar to patients with HD. zQ175 mice were crossbreed with CK2α' heterozygous mice (CK2α'$^{[+/-]}$) on the 129/SvEv-C57BL/6J background (Taconic Biosciences, RRID:IMSR_TAC:TF3062), originally obtained from Dr. Seldin (Boston University), for more than 20 generations. WT, zQ175, and zQ175:CK2α'$^{(+/-)}$ litter mates with mixed background 129/SvEv-C57BL/6J were used for the study. All mice were housed under standard SPF conditions. All experiments were performed according to procedures approved by the University of Minnesota Institutional Animal Care and Use Committee (Protocol #2001-38316A).

2.2 | Experimental design

A cohort of mice (WT $n = 13$, 8 females, 5 males; zQ175 $n = 16$, 7 females, 9 males; and zQ175:CK2α'$^{(+/-)}$ $n = 16$, 11 females, 5 males) were scanned at 3 months of age using a 9.4 T scanner, after which a subset of the animals ($n = 4$ per genotype) was killed for synapse density analyses ($n = 3$ per genotype were used). One additional zQ175:CK2α'$^{(+/-)}$ mouse was added to the cohort after the 3-month scan. The remaining animals were aged to 6 months at which time they were again scanned (WT $n = 9$, 7 females, 2 males; zQ175 $n = 12$, 5 females, 7 males; and zQ175:CK2α'$^{(+/-)}$ $n = 13$, 9 females, 4 males), and another subset ($n = 4$ per genotype) killed for synapse density analyses. Two zQ175:CK2α'$^{(+/-)}$ mice were harvested prior to being scanned at 12 months due to health issues. The remaining animals (WT $n = 5$ (3 females, 2 males), zQ175 $n = 8$ (4 females, 4 males), and zQ175:CK2α'$^{(+/-)}$ $n = 7$ (4 females, 3 males) were scanned at 12 months followed by striatal synapse density analyses (only $n = 3$ (2 females, 1 male) were used for zQ175:CK2α'$^{(+/-)}$ synapse analysis)). CK2α'$^{(+/-)}$ control mice were not included in the experimental design since they did not show significant changes in either T-S or C-S circuits compared to WT mice (Gomez-Pastor et al., 2017). We selected these three time points based on progression of motor symptoms (Heikkinen et al., 2012; Menalled et al., 2012): 3 months (pre-symptomatic), 6 months (early symptomatic) and 12 months (symptomatic). Sample sizes were estimated based on previous MRS studies of a similar nature (Heikkinen et al., 2012; Yu et al., 2022). Samples sizes for synapse density were estimated based on previous analyses of a similar nature (Gomez-Pastor et al., 2017; Zarate et al., 2021) and following standards recommended by Ippolito and Eroglu (2010). Longitudinal neuroimaging provided information for how neurochemical levels changed within individual mice over time. A diagram illustrating the experimental design is shown in Figure 1.

2.3 | Animal preparation for and monitoring during MR scanning

Experiments were conducted during the light cycle. Animals had unrestricted access to food and water. Animals were induced with 3% isoflurane (RRID:SCR_004098) in a 1:1 mixture of O_2:N_2O. Mice were secured in a custom-built mouse holder and physiological status was monitored (SA Instruments) and recorded. Anesthesia was maintained with 1.5–2% isoflurane to achieve a respiration rate of 70–100 breaths per minute. Body temperature was maintained at 36–37°C with a circulating warm water system and a heating fan controlled by feedback received from a fiber-optic rectal thermometer. The scan session was approximately 50 min for each animal. The experimenter was unaware of the experimental groups during data acquisition.

2.4 | MR protocol

All experiments were performed on a 9.4 T/31 cm scanner (Agilent, RRID:SCR_018054), as described previously (Friedrich et al., 2018; Öz et al., 2015). A quadrature surface radio frequency (RF) coil with two geometrically decoupled single-turn coils (14 mm diameter) was used as the MR transceiver. Following positioning of the mouse in the magnet, coronal and sagittal multislice images were obtained using a rapid acquisition with relaxation enhancement (RARE) sequence (Hennig et al., 1986) [repetition time (TR) = 4 s, echo train length = 8, echo time (TE) = 60 ms, slice thickness = 1 mm, 7 slices]. The volume of interest (VOI) was centered on the striatum (8.2 μl, $1.7 \times 2.0 \times 2.4\,mm^3$). The VOI size was chosen based on prior MRS studies in mouse models of HD, known striatal pathology in these models, as well as an ability to collect high-quality spectra with sufficient SNR. No indication of atrophy within the VOI was previously reported for the genotypes used in this study (Yu et al., 2022). All first- and second-order shims were adjusted using FASTMAP with echo-planar readout (Gruetter & Tkác, 2000). Localized ^{1}H MR spectra were acquired with a short-echo localization by adiabatic selective refocusing (LASER) sequence [TE = 15 ms, TR = 5 s, 256 transients] (Garwood & DelaBarre, 2001) combined with VAPOR (variable power RF pulses with optimized relaxation delays) water suppression (Tkác et al., 1999). Spectra were saved as single scans. Unsuppressed water spectra were acquired from the same VOI for metabolite quantification.

2.5 | Metabolite quantification

Single shots were eddy current, frequency and phase corrected using MRspa software (RRID:SCR_017292) (http://www.cmrr.umn.edu/downloads/mrspa/) before averaging. The contributions of individual metabolites to the averaged spectra were quantified using LCModel (Provencher, 1993) as described previously (Friedrich et al., 2018). The following metabolites were included in the basis set: alanine (Ala), ascorbate/vitamin C (Asc), aspartate, glycerophosphocholine (GPC), phosphocholine (PCho), creatine (Cr), phosphocreatine (PCr), gamma-aminobutyric acid (GABA), glucose (Glc), glutamine (Gln), glutamate (Glu), glutathione, glycine, *myo*-inositol (Ins), lactate (Lac), *N*-acetylaspartate (NAA), *N*-acetylaspartylglutamate (NAAG), phosphoethanolamine (PE), taurine (Tau), and macromolecules (MM). The MM spectra were experimentally obtained

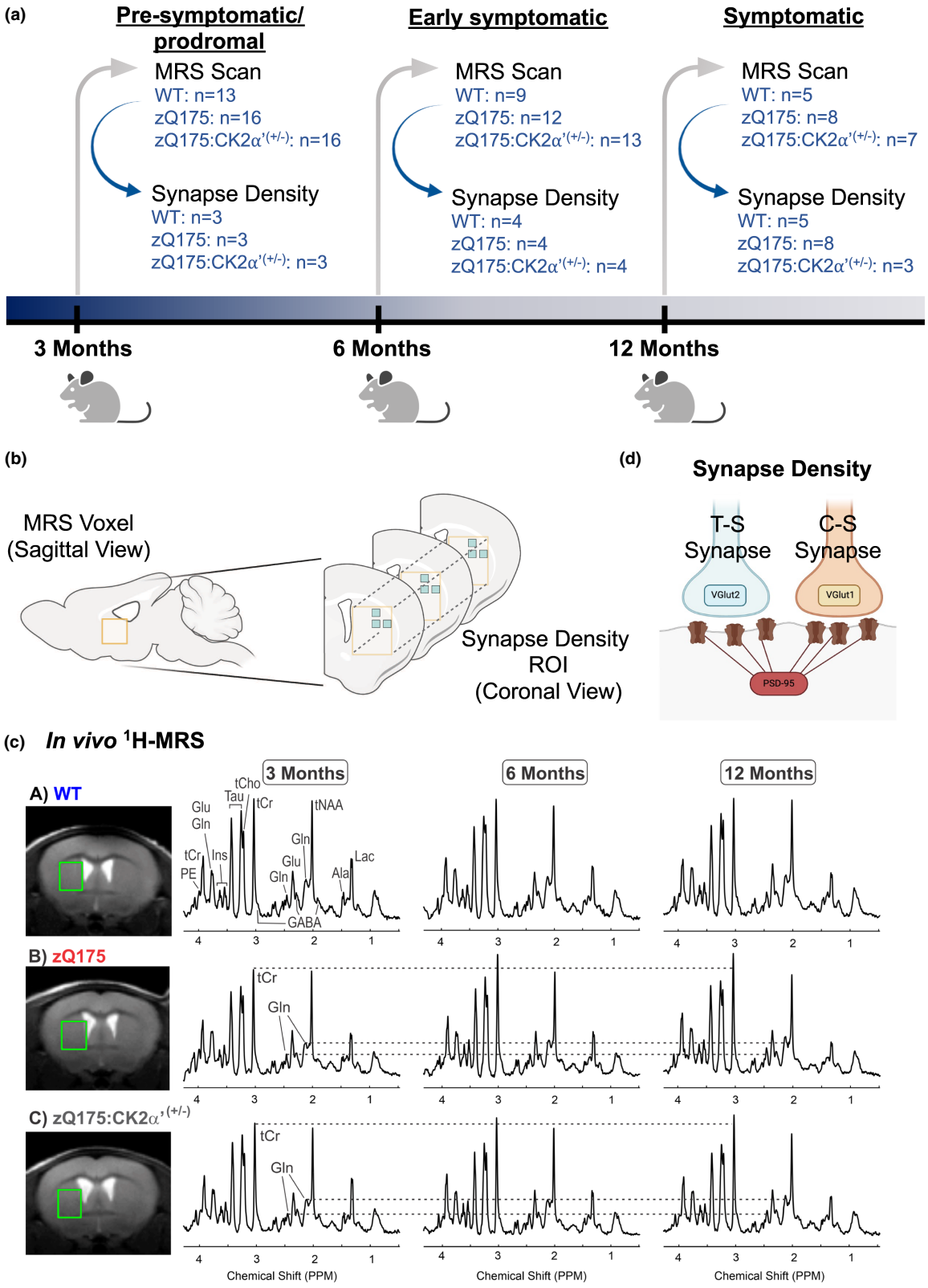

FIGURE 1 Diagram of experimental design and timeline. (a) Genotypes and number of animals used for each analysis are annotated. A cohort of WT, zQ175 and zQ175:CK2α$^{'(+/-)}$ mice were scanned longitudinally on a 9.4 T magnet (MRS) and a subset of mice were killed for synapse density analyses by immunohistochemistry at each time point. (b) Diagrams indicate the brain region covered by MRS and synapse analysis. Yellow box indicates voxel range (Volume = 8.2 μl), blue box indicates synapse density ROI within the voxel range. Synapse density was analyzed as described in the Methods and Materials section by conducting PSD-95 and VGlut1 or VGlut2 co-localization analyses from at least $n = 6$–9 images corresponding to $n = 3$ coronal sections. Graphics were created with Biorender.com (c) Localized proton MR spectra measured from the mouse dorsolateral striatum in WT, zQ175$^{(Tg/0)}$ and zQ175$^{(Tg/0)}$:CK2α$^{'(+/-)}$ mice at 3, 6, and 12 months old. The volume of interest is shown on T2-weighted images and alterations in neurochemicals visible in the spectra are shown.

from a VOI that covered the striatum using an inversion recovery technique [VOI = 4.7 ×2.1 ×2.7 mm^3, TE = 15 ms, TR = 2.0 s, inversion time (TIR) = 675 ms, 400 transients, $N = 2$]. The model metabolite spectra were generated using density matrix simulations (Govindaraju et al., 2000) with the MATLAB software (MathWorks, RRID:SCR_001622) based on previously reported chemical shifts and coupling constants (Govindaraju et al., 2000; Tkác, 2008). Metabolite concentrations were corrected for water and metabolite T_2 relaxation time and tissue water content. A water content of 82% was used. Concentrations were not corrected for CSF contribution to the VOI since there was no indication of atrophy within the VOI (Yu et al., 2022); also see Discussion. Concentrations with mean Cramér-Rao lower bounds (CRLB) ≤20% in any of the three groups were reported (Friedrich et al., 2018). If the correlation between two metabolites was consistently high (correlation coefficient $r < -0.7$), their sum was reported rather than the individual values (Friedrich et al., 2018), this was the case for total NAA (tNAA = NAA + NAAG), total Cr (tCr = Cr + PCr), and total Cho (tCho = GPC + PCho). In addition, Glc + Tau was reported in addition to the separate Glc and Tau concentrations because the Glc concentration did not always meet the mean CRLB ≤20% criterion and Glc and Tau have similar spectral patterns. Glu, Lac, NAA, Tau, tCr, tNAA, and Glc + Tau were quantified with mean CRLB <3%, GABA, Gln, Ins, and tCho were quantified with mean CRLB <6%, Ala, GSH, and PE were quantified with mean CRLB <10%, and Asc, and Gly were quantified with mean CRLB <14%.

2.6 | Animal sacrifice procedure

Mice were anesthetized with an Avertin stock solution (0.3125 g tribromoethanol [Sigma; T48402], 0.625 ml methylbutanol, 24.5 ml ddH2O). The use of Avertin is required when studying synapse density since other anesthetics such as isoflurane are known to alter PSD-95 levels and synapse density (Agarwal et al., 2022). Specific approval to use Avertin was obtained from IACUC (Protocol # 2007-38316A). The preparation of Avertin was conducted following IACUC guidelines. The solution was kept under refrigeration in the dark at pH~7 and it was replaced every 14 days. Induction with Avertin requires only 1–2 min and allows surgical anesthesia to last for 15–45 min with a sleep time of 60–120 min. A filtered sterile solution was administered by IP injection at a dose of 250 mg/Kg. This amounts to 0.5 ml of the described solution to a 25 g mouse. After confirmation of deep anesthesia by the absence of response to toe pinch and skin pinch mice were perfused intra-cardially with tris-buffered saline (TBS) (25 mM Tris-base, 135 mM Nacl, 3 mM KCl, pH 7.6) supplemented with 7.5 μM heparin followed with 4% PFA in TBS as previously described (Gomez-Pastor et al., 2017; Mckinstry et al., 2014). Brains were dissected, fixed with 4% PFA in TBS at 4 °C overnight, cryoprotected with 30% sucrose in TBS overnight and embedded in a 2:1 mixture of 30% sucrose in TBS:OCT (Tissue-Tek).

2.7 | Synapse density quantification

Two to three independent coronal brain sections were used for each mouse, containing the dorsal striatum (bregma 0.5–1.1 mm) and were stained with presynaptic VGlut1 (Millipore AB5905, 1:500, RRID:AB_2301751) or VGlut2 (Millipore, AB2251-I; 1:1000, RRID:AB_2665454) and post-synaptic PSD-95 (Thermo Fisher, 51–6900; 1:500; RRID:AB_2533914) markers as described previously (Gomez-Pastor et al., 2017; Ippolito & Eroglu, 2010; Mckinstry et al., 2014). Specificity and authentication of all primary antibodies have been previously tested using preabsorption of the VGlut1 antiserum with immunogen peptide, and in VGlut1 and VGlut2 KO-derived neuron/astrocyte cocultures (Li et al., 2013). Positive reactivity for PSD-95 antibody was confirmed on western blots of rat brain homogenates and lysates of PSD-95- transfected HEK293 cells (https://www.thermofisher.com/antibody/product/PSD-95-Antibody-Polyclonal/51-6900). Secondary antibodies used were goat anti-guinea pig Alexa 488 (VGlut1/2, Thermo Fisher Scientific A-11073, 1:200, RRID:AB_2534117) and goat anti-rabbit Alexa 594 (PSD-95, Thermo Fisher Scientific A-11012, 1:200, RRID:AB_2534079). At least three mice for each genotype; WT, zQ175, and zQ175:CK2α$'^{(+/-)}$ were evaluated. The confocal scans (optical section depth 0.34 mm, 15 sections per scan) of the synaptic zone in the dorsal striatum were performed at 60X magnification on an Olympus FV1000 confocal laser-scanning microscope (RRID:SCR_020337). Maximum projections of three consecutive optical sections were generated. The Puncta Analyzer Plugin for ImageJ (RRID:SCR_003070) was used to count co-localized synaptic puncta. The experimenter was blinded during experimentation and data analyses. This assay takes advantage of the fact that presynaptic and post-synaptic proteins reside in separate cell compartments (axons and dendrites, respectively), and they would appear to co-localize at synapses because of their close proximity. The number of animals used in this analysis was 3 per genotype (3 months), 4 per genotype (6 months), and 5–6 WT, 7–8 zQ175, and 3 zQ175:CK2α$'^{(+/-)}$ (12 months). The sample size was determined based on previous studies using a similar n (Gomez-Pastor et al., 2017; Ippolito & Eroglu, 2010; Mckinstry et al., 2014). Significant group differences were calculated using $n = 6–9$ images per animal resulting in a minimum of 18 data points per genotype for statistical analyses, as previously described (Gomez-Pastor et al., 2017; Zarate et al., 2021) and following recommendations by Ravalia et al. (2021).

2.8 | Data analysis

All statistics were conducted using GraphPad Prism 9 software (RRID:SCR_002798). Group averages between genotypes were compared at each time point using one-way ANOVA for MRS and synapse densities with Tukey's post hoc test to adjust for multiple comparisons. Significant group differences for synapse density were calculated using $n = 6–9$ images per animal, three animals minimum per genotype, resulting in a minimum of 18 data points per genotype for statistical

analyses. Only averages for each mouse are shown. Pearson correlation analyses were run separately for each neurochemical against synapse number. Holm–Šídák adjustment of correlation p-values was used to correct for the multiple testing of the many neurochemicals together with metabolite sums and metabolite ratio. A full report of results for MRS ANOVAs is in Table 1, with synapse analyses in Table 2, and correlation analyses in Table 3. To determine if there were age and/or genotype effects on correlations presented in Figure 4, multiple linear regressions were run for significant correlations (GABA, tCr, and PE) where each metabolite was regressed against age and genotype (metabolite ~ age + genotype + age:genotype). Pearson correlation coefficients between each regression's residuals and the corresponding synapse density were then calculated. Fisher's exact test was conducted to evaluate sex differences for all metabolites (none were found). No formal statistical assessment of normality was conducted. Outlier tests were not performed. For all statistical analyses, the P value threshold for significance was defined as $p < 0.05$. Adjusted p-values in Table 3 were determined using Holm-Šídák adjustment with an alpha set to 0.05. The defined threshold for significant correlations for C-S was $p < 0.0027$ and there were no significant adjusted p-values for T-S. Error bars always represent mean ± standard deviation (SD).

3 | RESULTS

3.1 | Longitudinal in vivo ^{1}H-MRS captures genotype and age-specific striatal neurochemical changes in the zQ175 HD mouse model

We utilized in vivo ^{1}H-MRS to measure neurochemicals in the striatum of WT, zQ175, and zQ175:CK2α$'^{(+/-)}$ mice in a longitudinal manner and in parallel with ex vivo synapse density analyses to obtain simultaneous information for potential neurochemical and synapse alterations across different genotypes and time points (Figure 1). A total of 19 neurochemicals, including four sums, were quantified reliably in the dorsolateral striatum (Table 1). In addition, tNAA/tCr ratio was computed as it is frequently utilized as a marker of neuronal viability and to enable comparison of the current results with prior literature. Seven neurochemicals (Ala, Asc, Gln, Ins, PE, tCho, and tCr) and tNAA/tCr showed significant group differences primarily at 6 and 12 months of age (Figure 2). Ala, Asc, Ins, and PE (Figure 2a–d) showed a decrease with age in WT mice while Gln (Figure 2e) increased. Similar age-dependent alterations in brain neurochemicals have also been reported in C57BL/6 mice and in human studies comparing young and middle-aged subjects (Duarte et al., 2014; Grachev & Apkarian, 2001), indicating these alterations are common brain modifications during aging.

The levels of several neurochemicals in zQ175 mice significantly differed compared to WT at multiple time points. Gln was significantly higher in zQ175 versus WT started at 3 months and increased even further at 6 and 12 months (Figure 2e). tCr was significantly higher and tCho lower in zQ175 mice versus WT at 6 and 12 months (Figure 2f,g) coinciding with previously reported worsening motor and cognitive symptoms. On the other hand, no significant differences in tNAA were observed between WT and zQ175 mice while a higher Ins level in zQ175 mice reached statistical significance only at 6 months (Figure 2d, Table 1), recapitulating what was previously reported for this mouse model (Heikkinen et al., 2012). When tNAA was referenced to tCr, which is often used as an internal concentration reference, we found a significantly lower (tNAA/tCr) ratio in zQ175 versus WT mice at 6 and 12 months (Figure 2h). This ratio was relatively stable in WT mice over time, but it showed an age-dependent decrease in zQ175 mice. However, this alteration most likely reflects changes in tCr. On the other hand, changes in Gln, tCr, tCho, and tNAA/tCr in HD mice coincided with symptom onset and progression for this HD mouse model. No sex differences were observed among the genotypes in our dataset.

Given the previously described positive effects of CK2α' haploinsufficiency in ameliorating HD-like symptoms (Gomez-Pastor et al., 2017; Yu et al., 2022), we expected to see a number of neurochemicals that were significantly different between zQ175 and zQ175:CK2α$'^{(+/-)}$ mice. Interestingly, we only observed significant differences between these two genotypes at 3 months for Gln (Figure 2e), while no significant differences were observed between WT and zQ175:CK2α$'^{(+/-)}$ mice at the later time points.

3.2 | Loss of thalamo-striatal excitatory synapses precedes cortico-striatal synapse loss and is sustained over time

To study whether specific neurochemical alterations relate to changes in synapse density, we first determined changes in excitatory synapse density in WT, zQ175, and zQ175:CK2α$'^{(+/-)}$ mice, looking at both C-S and T-S circuitries during disease progression (Figure 3a). Synapse density was quantified using immunofluorescent colocalization of the presynaptic markers VGlut1 (Vesicular glutamate transporter 1: specific marker for cortical input) and VGlut2 (Vesicular glutamate transporter 2: specific marker for thalamic input) (Fujiyama et al., 2004; Huerta-Ocampo et al., 2014) and the post-synaptic marker PSD-95 (post-synaptic density protein 95) in the dorsal striatum of 3-, 6-, and 12-month-old animals (Figure 3b). C-S synapses were initially higher in zQ175:CK2α$'^{(+/-)}$ mice compared to WT, however by 6 months this trend had reversed and by 12 months had become significantly lower in both zQ175 and zQ175:CK2α$'^{(+/-)}$ mice compared to WT (Figure 3c, Figure S1, Table 2). In contrast, levels of T-S synapses in zQ175 mice were significantly reduced compared to WT at all three time points while these decreases were significantly rescued in zQ175:CK2α$'^{(+/-)}$ mice at 3 and 6 months (Figure 3d, Figure S1, Table 2).

3.3 | Changes in striatal neurochemical levels correlate with circuit-dependent changes in synapse density

Given the alterations in neurochemical levels and changes in excitatory synapse densities between the different genotypes, we wanted

TABLE 1 ANOVA results for neurochemical concentrations measured by ^{1}H-MRS

µmol/g (mean ± SD)												
	3 Months				6 Months				12 Months			
Metabolite	WT	zQ175	zQ175:CK2α′$^{(+/-)}$	*p*-value	WT	zQ175	zQ175:CK2α′$^{(+/-)}$	*p*-value	WT	zQ175	zQ175:CK2α′$^{(+/-)}$	*p*-value
Ala	1.64 ± 0.31	1.5 ± 0.29	1.5 ± 0.37	ns	1.21 ± 0.24	0.89 ± 0.21	1.06 ± 0.22	**0.0071	0.97 ± 0.33	0.81 ± 0.32	0.90 ± 0.09	ns
Asc	1.33 ± 0.27	1.32 ± 0.20	1.28 ± 0.30	ns	1.30 ± 0.26	1.44 ± 0.36	1.52 ± 0.26	ns	1.10 ± 0.24	1.45 ± 0.44	1.74 ± 0.45	#0.0389
Asp	n/a	1.52 ± 0.46	1.39 ± 0.28	ns	1.56 ± 0.49	1.46 ± 0.41	1.57 ± 0.38	ns	n/a	1.60 ± 0.31	n/a	ns
GABA	2.59 ± 0.41	2.69 ± 0.26	2.74 ± 0.30	ns	2.49 ± 0.26	2.59 ± 0.27	2.59 ± 0.28	ns	2.48 ± 0.14	2.40 ± 0.29	2.43 ± 0.37	ns
Glc	2.49 ± 1.04	n/a	2.24 ± 0.89	ns	2.68 ± 0.60	2.87 ± 0.96	1.72 ± 0.63	#0.0228 ◆◆0.0019	n/a	n/a	n/a	ns
Gln	2.95 ± 0.20	3.16 ± 0.15	2.87 ± 0.26	*0.0259 ◆◆ ◆ 0.0009	3.06 ± 0.10	3.36 ± 0.24	3.21 ± 0.27	*0.0143	3.46 ± 0.25	4.12 ± 0.35	3.79 ± 0.26	**0.0031
Glu	6.86 ± 0.51	7.07 ± 0.40	6.82 ± 0.45	ns	7.01 ± 0.54	7.11 ± 0.30	7.04 ± 0.51	ns	7.24 ± 0.46	7.06 ± 0.60	7.15 ± 0.23	ns
GSH	0.98 ± 0.08	0.99 ± 0.11	1.04 ± 0.12	ns	1.11 ± 0.16	1.00 ± 0.16	0.96 ± 0.13	ns	0.88 ± 0.10	0.78 ± 0.27	0.87 ± 0.15	ns
Gly	1.01 ± 0.17	0.94 ± 0.24	1.04 ± 0.13	ns	1.00 ± 0.15	1.12 ± 0.17	1.09 ± 0.25	ns	0.84 ± 0.27	1.05 ± 0.32	1.11 ± 0.25	ns
Ins	3.70 ± 0.36	4.10 ± 0.52	3.95 ± 0.41	ns	3.72 ± 0.32	4.24 ± 0.49	4.16 ± 0.24	**0.0076 #0.0234	3.41 ± 0.38	3.89 ± 0.48	3.98 ± 0.39	ns
Lac	6.54 ± 0.96	6.21 ± 0.86	6.48 ± 1.00	ns	5.56 ± 1.36	5.02 ± 0.93	5.60 ± 0.69	ns	5.50 ± 1.63	4.76 ± 1.46	5.06 ± 0.85	ns
NAA	6.15 ± 0.19	6.11 ± 0.18	6.05 ± 0.23	ns	6.13 ± 0.16	6.13 ± 0.21	6.01 ± 0.21	ns	6.36 ± 0.23	6.10 ± 0.31	6.03 ± 0.41	ns
PE	2.64 ± 0.42	2.60 ± 0.41	2.54 ± 0.23	ns	2.61 ± 0.34	2.13 ± 0.42	2.17 ± 0.30	*0.0129 # 0.0218	2.25 ± 0.21	2.17 ± 0.15	2.04 ± 0.30	ns
Tau	13.47 ± 1.14	13.02 ± 0.79	13.01 ± 0.73	ns	12.87 ± 0.42	12.34 ± 0.92	12.14 ± 0.60	ns	13.08 ± 1.16	12.31 ± 1.27	12.56 ± 0.76	ns
tCho	1.47 ± 0.13	1.4 ± 0.11	1.32 ± 0.08	##0.0027	1.54 ± 0.12	1.39 ± 0.14	1.31 ± 0.10	*0.0242 ### 0.0005	1.51 ± 0.04	1.32 ± 0.16	1.34 ± 0.09	*0.0354
tCr	7.54 ± 0.22	7.62 ± 0.19	7.55 ± 0.20	ns	7.71 ± 0.35	8.35 ± 0.25	8.17 ± 0.24	****<0.0001 ##0.0015	7.54 ± 0.32	8.48 ± 0.63	8.52 ± 0.31	**0.0076 ##0.0069
tNAA (NAA + NAAG)	6.39 ± 0.22	6.34 ± 0.18	6.32 ± 0.27	ns	6.39 ± 0.18	6.34 ± 0.24	6.26 ± 0.28	ns	6.62 ± 0.28	6.38 ± 0.28	6.26 ± 0.43	ns
Glc + Tau	15.76 ± 2.16	15.41 ± 1.48	15.25 ± 1.22	ns	15.25 ± 0.93	15.22 ± 1.63	13.86 ± 0.88	#0.0340 ◆0.0239	14.78 ± 1.98	14.60 ± 2.31	14.00 ± 1.48	ns
tNAA/tCr	0.85 ± 0.03	0.83 ± 0.03	0.84 ± 0.03	ns	0.83 ± 0.04	0.76 ± 0.03	0.77 ± 0.03	***0.0002 ## 0.0005	0.88 ± 0.04	0.75 ± 0.06	0.74 ± 0.06	**0.0047 ##0.0018

Note: Neurochemical concentrations in WT, zQ175, and zQ175:CK2α′$^{(+/-)}$ mice over time. Values represented as mean ± SD. One-way ANOVA with Tukey-adjusted *p*-values for those <0.05. *Indicates WT vs. zQ175, #Indicates WT vs. zQ175:CK2α′$^{(+/-)}$, and ◆Indicates zQ175 vs. zQ175:CK2α′$^{(+/-)}$. For 3 month WT $n = 13$, zQ175 $n = 16$, zQ175:CK2α′$^{(+/-)}$ $n = 16$. 6 month WT $n = 9$, zQ175 $n = 12$, zQ175:CK2α′$^{(+/-)}$ $n = 13$. 12 month WT $n = 5$, zQ175 $n = 8$, zQ175:CK2α′$^{(+/-)}$ $n = 7$.

TABLE 2 Excitatory synapse density ANOVA results

	3 months		6 Months		12 Months	
	Mean Synapse Density (per 15.42 mm^2)	Tukey-Adjusted, *p*-value	Mean Synapse Density (per 15.42 mm^2)	Tukey-Adjusted, *p*-value	Mean Synapse Density (per 15.42 mm^2)	Tukey-Adjusted, *p*-value
C-S Synapses						
WT vs. zQ175	643.9 ± 259.6 vs. 714.1 ± 201.5	0.5769	995.0 ± 376.7 vs. 861.6 ± 291.4	0.1976	705.8 ± 226.4 vs. 430.2 ± 103.3	<0.0001
WT vs. zQ175:CK2α$^{(+/-)}$	643.9 ± 259.6 vs. 874.6 ± 276.0	0.0031	995.0 ± 376.7 vs. 806.9 ± 273.9	0.0425	705.8 ± 226.4 vs. 428.7 ± 151.2	<0.0001
zQ175 vs. zQ175:CK2α$^{(+/-)}$	714.1 ± 201.5 vs. 874.6 ± 276.0	0.0628	861.6 ± 291.4 vs. 806.9 ± 273.9	0.7661	430.2 ± 103.3 vs. 428.7 ± 151.2	0.4791
T-S Synapses						
WT vs. zQ175	384.5 ± 110.1 vs. 303.0 ± 83.37	0.0134	351.4 ± 153.3 vs. 210.9 ± 143.8	0.0072	323.8 ± 147.0 vs. 237.1 ± 88.44	0.0060
WT vs. zQ175:CK2α$^{(+/-)}$	384.5 ± 110.1 vs. 390.1 ± 88.26	0.9778	351.4 ± 153.3 vs. 396.5 ± 256.6	0.5921	323.8 ± 147.0 vs. 288.9 ± 253.9	0.5932
zQ175 vs. zQ175:CK2α$^{(+/-)}$	303.0 ± 83.37 vs. 390.1 ± 88.26	0.0083	210.9 ± 143.8 vs. 396.5 ± 256.6	0.0003	237.1 ± 88.44 vs. 288.9 ± 253.9	0.2900

Note: Mean raw synapse density per 15.42 mm^2 between genotypes and across time points. Error presented as ± SD. One-way ANOVA with Tukey-adjusted *p*-values. At each time point, WT $n = 3–6$, zQ175 $n = 3–8$, zQ175:CK2α$^{(+/-)}$ $n = 3–4$. Significant group differences were calculated using $n = 6–9$ images per animal.

to determine if these two measures were significantly correlated with each other, potentially allowing us to identify neurochemical markers for synapse loss in HD. We performed correlation analyses across all mice used in this study ($n = 36$). Synapse number for each mouse analyzed at one of three time points (3, 6, and 12 months) was used as the predictor variable in the analysis and neurochemical levels at the same time points as the response variable (Figure 4, Table 3). Regressions were run separately to examine each synaptic circuit, T-S and C-S, and their correlation with each neurochemical level. When analyzed in this manner, we found a significant positive correlation ($p < 0.05$) between C-S synapse number and GABA (Figure 4a,b). The statistical significance of this correlation was maintained even after conservative multiple testing adjustment of *p*-values across all the metabolites. Gln and tCho had statistically significant unadjusted p-values but only modestly sized correlations. It is important to note that despite the positive correlation between GABA and C-S synapse number, we did not observe a reduction in GABA levels in the two HD models relative to WT (Table 1).

In T-S circuitry, we found two neurochemicals (PE and tCr) correlated with T-S synapse density. PE had a positive correlation of a meaningful magnitude (Table 3, Figure 4c–g) while tCr had a slightly weaker correlation value. Conservative multiple testing adjustment of p-values across all the metabolites did not maintain their statistical significance despite the global effect being significant. This could be because of the conservatism of the multiple testing adjustment, the high number of MRS measurements being tested ($n = 20$), and the relatively small sample size which together may result in rejecting significant associations that in reality are meaningful. Among the neurochemicals that showed significant correlations with synapse density based on unadjusted p-values, PE was significantly lower in both zQ175 and zQ175:CK2α$^{(+/-)}$ than WT at 6 months (Figure 2c, Table 1), while tCr showed an increasing trend over time in both zQ175 and zQ175:CK2α$^{(+/-)}$ and was higher than WT at 6 and 12 months (Figure 2f). This data indicate that by combining the levels of GABA, PE, and tCr, it could be possible to evaluate circuit-dependent synapse content in HD.

In order to address age and/or genotype effects on the correlations, we performed multiple linear regression analyses on metabolite concentrations regressed against age and genotype (metabolite ~ age + genotype + age:genotype). We then used the residuals from the regression results, which indicate any leftover variation that cannot be explained by age and/or genotype and performed correlations with synapse number to determine if changes in metabolites could be explained by synapse number alone without age or genotype effects (Figure S2). We found these correlations between synapse number and metabolite showed that C-S synapses against GABA were significantly correlated ($p = 0.0036$). This is interpreted as the correlation between GABA and C-S synapses is not influenced by age and/or genotype. In the case of metabolites associated with T-S synapses, we found the residuals to be not significant for these metabolites (PE, $p = 0.3559$; tCr, $p = 0.7544$), which indicate that a contribution of age and/or genotype to the correlations observed between these neurochemicals and T-S synapse density is plausible.

TABLE 3 Correlation analyses between raw synapse number and metabolite concentration

	T-S Synapse #			C-S Synapse #		
Metabolite	Pearson's r	Unadjusted *p*-value	Adjusted *p*-value	Pearson's r	Unadjusted *p*-value	Adjusted *p*-value
Ala	0.3108	0.065	0.6810	−0.07708	0.6648	0.9942
Asc	0.06893	0.6896	0.9995	−0.1922	0.2762	0.9793
Asp	−0.02084	0.904	0.9995	0.1269	0.4745	0.9942
GABA	−0.2257	0.1856	0.9307	0.5867	0.0003	0.0057
Glc	−0.1076	0.5321	0.9995	0.2246	0.2015	0.9658
Gln	−0.2463	0.1477	0.9090	−0.346	0.045	0.5634
Glu	−0.2434	0.1526	0.9090	0.09244	0.6031	0.9942
GSH	0.09119	0.5968	0.9995	0.2216	0.2078	0.9658
Gly	−0.1083	0.5294	0.9995	0.1223	0.4907	0.9942
Ins	−0.09496	0.5817	0.9995	0.08881	0.6174	0.9942
Lac	0.262	0.1227	0.8769	−0.2056	0.2435	0.9734
NAA	−0.149	0.3859	0.9953	0.1599	0.3662	0.9895
PE	0.3416	0.0415	0.5531	−0.04997	0.779	0.9942
Tau	0.02923	0.8656	0.9995	0.1849	0.2951	0.9793
tCho	0.01158	0.9466	0.9995	0.3392	0.0497	0.5796
tCr	−0.3315	0.0483	0.5898	−0.1056	0.5523	0.9942
tNAA (NAA + NAAG)	−0.08544	0.6203	0.9995	0.07763	0.6626	0.9942
Glc + Tau	−0.05712	0.7407	0.9995	0.2565	0.1431	0.9155
tNAA/tCr	0.2137	0.2109	0.9417	0.1401	0.4295	0.9936

Note: Pearson coefficient and unadjusted *p*-value calculated from correlation analyses between all neurochemicals and raw synapse # (C-S and T-S correlations run separately). Holm-Šídák multiple comparison post-hoc test was run for C-S and T-S separately, represented by adjusted *p*-values. All ages and genotypes are pooled for each analysis corresponding to WT $n = 12$, zQ175 $n = 15$ and zQ175:CK2α′$^{(+/-)}$ $n = 9$ from all three time points (3, 6 and 12 months).

Since no significant changes were observed in T-S synapse density in WT mice with age (Figure S1), we suggest that the correlations between T-S synapse density and PE and tCr are most likely influenced by genotype.

4 | DISCUSSION

In this first direct assessment of the longitudinal association between neurochemical abnormalities and excitatory synapse density in the mouse brain, we show that distinct neurochemical levels significantly correlate with different striatal glutamatergic synaptic input pathways in the zQ175 model, suggesting that ^{1}H-MRS may distinguish circuit-dependent synapse changes in HD.

The current immunofluorescence data confirmed and expanded previous observations regarding changes in T-S and C-S synapse density in zQ175 and other mouse models (Deng et al., 2014; Gomez-Pastor et al., 2017; Mckinstry et al., 2014; Raymond et al., 2011) and showed that C-S synapse depletion occurs at advanced disease stages in fully symptomatic animals, while T-S synapse depletion occurs earlier. We also showed that reducing levels of CK2α', a kinase previously associated with the dysregulation of synaptic activity in HD (Gomez-Pastor et al., 2017; Yu et al., 2022), prevented loss of T-S synapses, at least during the first 6 months of life, without altering C-S synapse density, supporting previous data in younger mice (Gomez-Pastor et al., 2017). However, in older mice (12 months), no significant differences were observed between WT and zQ175:CK2α′$^{(+/-)}$ or between zQ175 and zQ175:CK2α′$^{(+/-)}$ groups. Taken together, these data further demonstrate that there are age-dependent and circuit-specific changes in striatal excitatory synapse dysfunction in HD that, in the T-S pathway, are in part ameliorated by reducing levels of CK2α'. It remains unknown how CK2α' haploinsufficiency selectively improved T-S synapse loss during the early stages of disease, although this could be related to a different regulatory role of CK2α' between D1 and D2-MSNs, the latter being preferentially altered in HD (Rebholz et al., 2013; Reiner et al., 1988). Further studies are warranted to uncover the specific role of CK2α' in the differential regulation of T-S and C-S synapses.

^{1}H-MRS in patients with SCAs with different degrees of synapse loss showed a similar ranking in the severity of neurochemical alterations suggesting that neurochemical abnormalities across different SCAs, and perhaps other neurodegenerative diseases, may reflect abnormalities in synaptic function or density (Joers et al., 2018; Öz, Vollmers, et al., 2011). Immunohistochemical analyses for synaptic vesicles (SV2A) combined with antemortem ^{1}H-MRS in brains from patients with Alzheimer's disease (AD) showed decreased tNAA/tCr

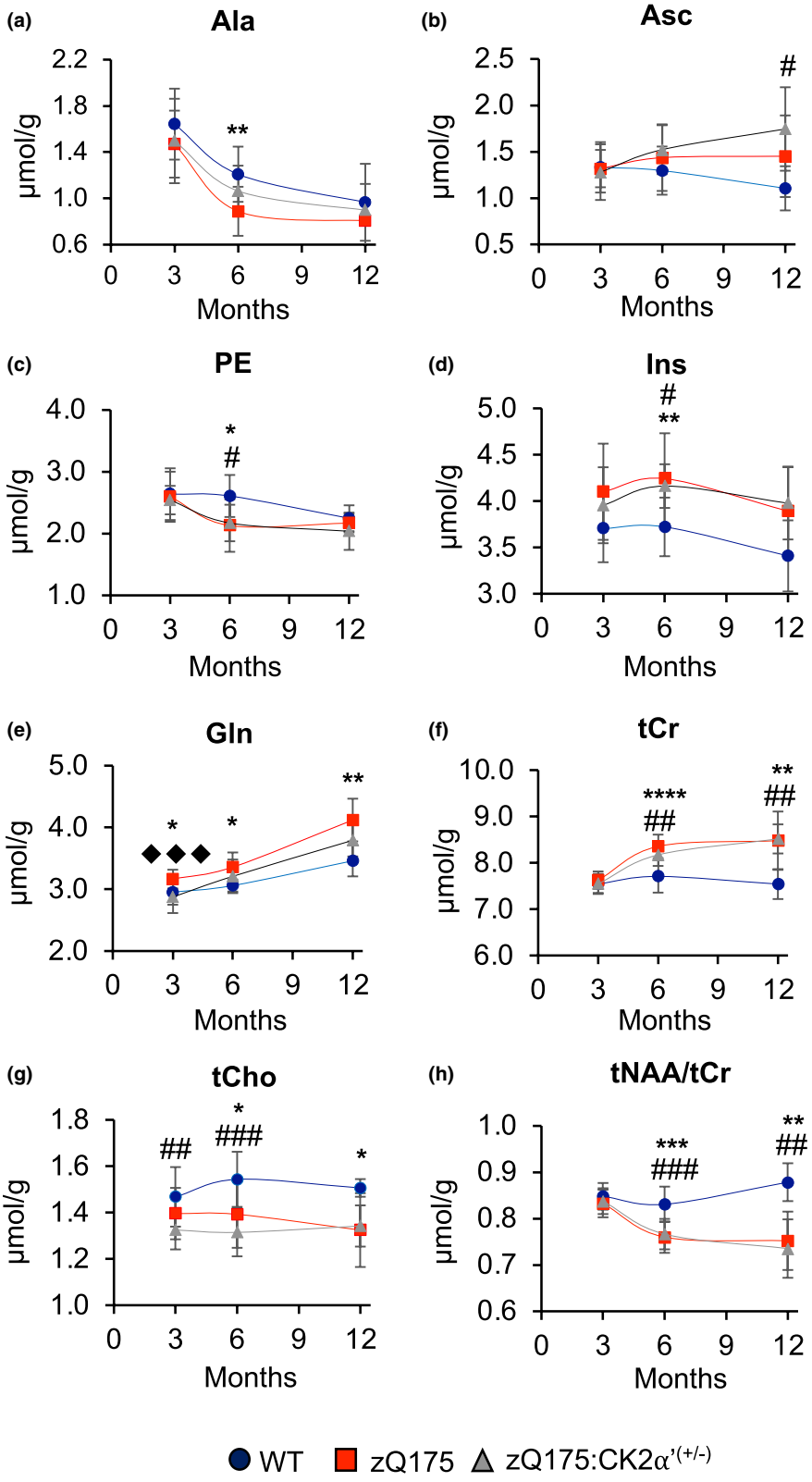

FIGURE 2 Age and genotype-dependent neurochemical alterations in the mouse dorsolateral striatum. Longitudinal metabolite profile in WT, zQ175, and zQ175:CK2α'$^{(+/-)}$ mice. Only neurochemicals that showed significant differences between genotypes are shown (see Table 1). Error bars represent mean ± SD. One-way ANOVA with Tukey's post hoc test. *$p < 0.05$ WT versus zQ175, #$p < 0.05$ WT versus zQ175:CK2α'$^{(+/-)}$, ♦$p < 0.05$ zQ175 versus zQ175:CK2α'$^{(+/-)}$. Abbreviations can be found in the methods section. For 3-month WT $n = 13$, zQ175 $n = 16$, zQ175:CK2α'$^{(+/-)}$ $n = 16$. 6-month WT $n = 9$, zQ175 $n = 12$, zQ175:CK2α'$^{(+/-)}$ $n = 13$. 12-month WT $n = 5$, zQ175 $n = 8$, zQ175:CK2α'$^{(+/-)}$ $n = 7$.

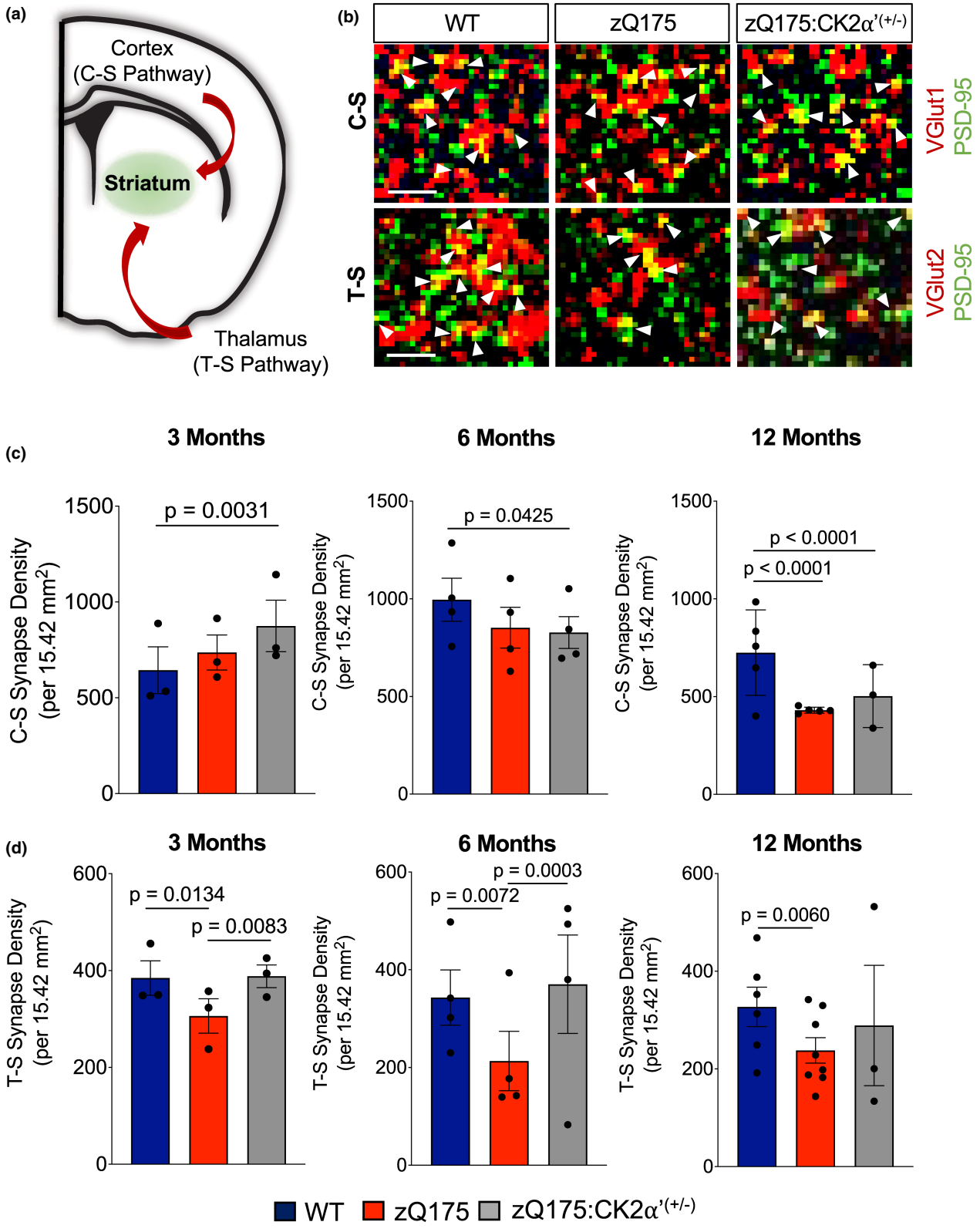

FIGURE 3 Onset of thalamo-striatal (T-S) synapse loss precedes cortico-striatal synapse deficits in zQ175 mice and it is delayed in zQ175:CK2α'$^{(+/-)}$ mice. (a) Diagram of the striatal excitatory circuitry. (b) Colocalization (white arrows) of pre-synaptic (VGlut1/2) and post-synaptic (PSD-95) markers in WT, zQ175, and zQ175:CK2α'$^{(+/-)}$ mice. Representative images from 6 months, total area analyzed was 15.42 mm^2. Scale bar: 5 μm. (c, d) Quantification of raw C-S and T-S synapse density number, respectively, at 3, 6, and 12 months old between genotypes. At each time point, WT $n = 3–6$, zQ175 $n = 3–8$, zQ175:CK2α'$^{(+/-)}$ $n = 3–4$. Data points represent biological replicates. Statistics were calculated using $n = 6–9$ images per animal. Error bars represent mean ± SD. $^*p < 0.05$, $^{**}p < 0.01$, $^{***}p < 0.001$, $^{****}p < 0.0001$, one-way ANOVA with Tukey's post hoc test.

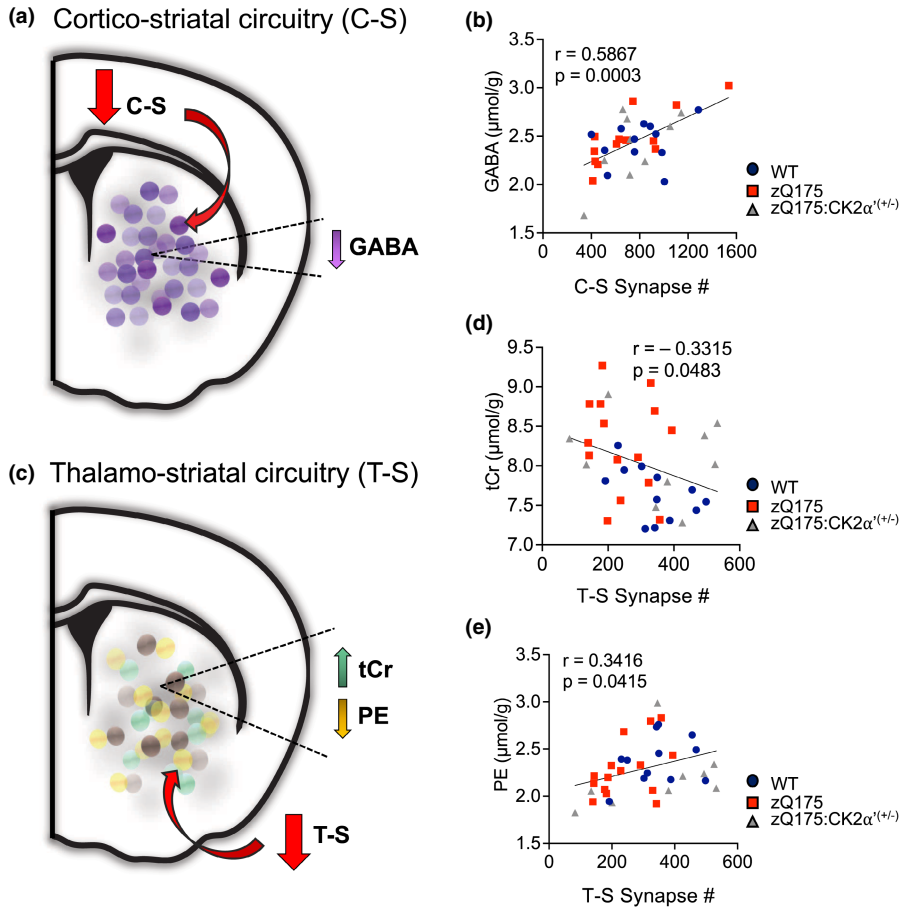

FIGURE 4 Selective neurochemical alterations differentially correlate with striatal synaptic circuits. (a) Illustration of C-S correlation with metabolites (GABA). (b) Correlation analysis of C-S synapse density versus GABA where raw synapse numbers are plotted against corresponding neurochemical levels. (c) Illustration T-S correlation with metabolites (tCr and PE). (d, e) Correlation analysis of neurochemicals versus T-S synapse density. *r* value represents Pearson's correlation. Data from WT $n = 12$, zQ175 $n = 15$, zQ175:CK2α$^{'(+/-)}$ $n = 9$ corresponding to all three time points (3, 6 and 12 months) is shown.

was associated with loss of synapses and early Tau pathology while increased Ins/tCr was associated with the occurrence of amyloid plaques in AD (Murray et al., 2014). Furthermore, a recent study in an AD mouse model with engrafted WT neural stem cells in the hippocampus showed changes in NAA and Glu that paralleled altered expression of synaptic proteins like PSD-95 and synaptophysin, and number of synapses (measured by electron microscopy) (Zhang et al., 2017). In a different study, ^{1}H-MRS and synaptic protein analyses by immunoblotting in mice fed with a high-fat diet showed increases in tCr and Gln that paralleled decreased synaptic proteins PSD-95 and VGlut1 (Lizarbe et al., 2018). Although correlations between neurochemicals and synapse numbers were not investigated with data collected in the same brains at the same time point/age in these prior studies, these reports established a plausible connection between key neurochemical alterations and synapse density.

In HD, ^{1}H-MRS analyses have highlighted tNAA, Ins, and tCr as neurochemical markers of neurodegeneration (Heikkinen et al., 2012; Peng et al., 2016; Sturrock et al., 2010, 2015; Tkác et al., 2007). However, the differences between HD mouse models and patients regarding alterations of these specific neurochemicals necessitate a careful analysis and validation of their potential relevance in defining synapse loss. In pre-symptomatic patients with HD, tNAA is lower than unaffected individuals and decreases further during disease progression, correlating with impaired motor and cognitive function (Leavitt et al., 2011). Lower NAA and higher Ins were previously reported only in symptomatic HD mouse models with severe progression such as the R6/2 (12 weeks) and the homozygous zQ175$^{(Tg/Tg)}$ (12 months), and in older zQ175 $^{Tg/0}$ (22 months) (Heikkinen et al., 2012; Peng et al., 2016; Tkác et al., 2007; Yu et al., 2022). On the contrary, longitudinal MRS performed at 7 T in zQ175, showed no significant alterations in tNAA or Ins up to 12 months (Heikkinen et al., 2012). Therefore, these data suggest that changes in tNAA and Ins in HD mice may reflect substantial neurodegeneration only in advanced disease. Our current data at 9.4 T validated the absence of alterations for tNAA up to 12 months. In addition, we found higher Ins in zQ175 versus WT mice, which was significant at 6 months. Discrepancies between HD mouse models and patients were also reported for tCr (Adanyeguh et al., 2018; Sánchez-Pernaute et al., 1999; Sturrock et al., 2015). We confirmed an age-dependent increase in tCr in zQ175 and reported additional

alterations in Gln, tCho, and tNAA/tCr between WT and zQ175. These changes were not attributed to ventricular enlargement or large brain volume alterations between zQ175 and WT mice since no differences in these parameters were observed even in older mice (Yu et al., 2022). Also, if CSF contribution to the MRS voxel was significantly higher in HD versus WT mice, we would expect a lowering of all metabolite levels in HD versus WT, however some metabolites are higher (e.g., tCr, Gln, Ins) while others (tCho, PE, Ala) are lower in HD versus WT. We conclude that Gln, tCr, tCho, and tNAA/tCr represent neurochemical markers that monitor disease progression in zQ175 mice better than tNAA or Ins.

Among all tested neurochemicals, we only detected a significant alteration in Gln when comparing zQ175 and zQ175:CK2α'$^{(+/-)}$. This was unexpected because of this latest model showing improvements in several HD-like phenotypes including decreased HTT aggregation and astrogliosis, increased synaptic density and neuronal excitability, and improved motor coordination (Gomez-Pastor et al., 2017; Yu et al., 2022). Gln levels increased over time in all mice but were significantly higher in zQ175 compared to WT starting at 3 months, consistent with a previously reported excitotoxic state (Fan & Raymond, 2007; Hassel et al., 2008). Analyses in R6/2 mice showed early increases in Gln levels (Tkác et al., 2007). Increased Gln has been associated with an imbalance in Glu-Gln cycling between neurons and astrocytes, reflecting compromised glutamatergic neurotransmission (Behrens et al., 2002; Liévens et al., 2001). Notably, no significant difference in Gln levels was found between WT and zQ175:CK2α'$^{(+/-)}$, indicating that the characteristic increase in Gln in zQ175 could be delayed as a consequence of manipulating CK2α' levels. Therefore, it is reasonable to hypothesize that early decreased Gln in zQ175:CK2α'$^{(+/-)}$ versus zQ175 could be associated with improved neuronal excitability. In support of this hypothesis, zQ175:CK2α'$^{(+/-)}$ previously showed improved AMPA-mediated excitatory transmission in the dorsolateral striatum when compared with zQ175 (Yu et al., 2022). Correlation analyses revealed a direct association between changes in specific neurochemicals and circuit-dependent synapse changes. We found a significant positive correlation between levels of GABA and C-S synapse density. GABA is known for its role as the primary inhibitory neurotransmitter in the adult brain and dysfunction in GABAergic signaling has been implicated in HD and other movement disorders (Hsu et al., 2018). Lower GABA content in the dorsal striatum and cortex was reported in postmortem brain from patients with HD (Spokes et al., 1980). Metabolic profiling using ^{13}C labeling and mass spectrometry in symptomatic R6/2 mice also showed decreased GABA synthesis (Skotte et al., 2018). However, ^{1}H-MRS did not reveal changes in GABA levels in R6/2 compared with WT (Tkác et al., 2007). We also did not detect significant differences in the average GABA concentration between WT and zQ175. A potential explanation is that ANOVAs of the neurochemical concentrations are based on the average concentration across multiple mice within the same genotype and the variability within groups overwhelmed the group differences across genotypes. However, the correlation analyses are conducted by plotting individual concentrations for each analyzed animal and their corresponding C-S synapse number. Therefore, the discrepancy between the lack of overall alterations in GABA and its correlation with C-S synapse density may reflect individual levels of GABA are inherently associated with C-S synapse density regardless of genotype or age. This is supported by correlation analyses performed with the residuals obtained from the regression analyses comparing metabolite concentrations against age and genotype, which suggested that the correlation between GABA and C-S synapses is not influenced by age and/or genotype.

On the other hand, we observed significant correlations between T-S synapse density and PE, and tCr. Alterations in PE and tCr, which are connected with neuronal integrity and function, have been consistently reported in mouse models and patients with HD and are associated with disease burden (Adanyeguh et al., 2018; Sturrock et al., 2010, 2015; Tkác et al., 2007). tCr increased over time in zQ175 and zQ175:CK2α'$^{(+/-)}$ compared with WT and significantly correlated with T-S synapse density. Contrary to GABA, the metabolites associated with T-S synapses (PE and tCr), were influenced by age and/or genotype. Because no significant changes were observed in T-S synapse density in WT with age, we concluded that the correlations between T-S synapse density and PE and tCr could be representative of genotype effects. Therefore, our data suggest that a combination of the levels of GABA, PE, and tCr could be used as neurochemical correlates to assess levels of striatal glutamatergic synapses in HD.

Overall, this study demonstrates the preliminary feasibility of using ^{1}H-MRS to potentially monitor synaptic changes in vivo during HD progression. One important aspect to consider here is the translational potential of this work into humans. While translation from studies conducted in different models of HD into humans is challenging, the similarities found in the pathophysiology between zQ175 and patients with HD thus hold the most promise in terms of translational potential. To further evaluate the translational potential of MRS in monitoring synapse density in patients several limitations need to be addressed in future studies. First, the MRS volume is larger than the area covered in synapse density analyses. The correlation analyses could be improved in future studies by reducing the MRS VOI size and distributing the tissue sampling areas for immunohistochemistry further within the MRS VOI. Second, the significant correlations between neurochemicals and synapse density may be influenced by other neuropathological features, relatively small sample size, or age. Finally, although our data did not reveal any sex differences in neurochemicals or synapse density, we cannot exclude a contribution of sex if a higher sample size is studied, considering that sex differences in brain development were found in zQ175 (Peng et al., 2016; Zhang et al., 2020). Therefore, further studies are needed to corroborate these preliminary findings in alternative models of HD to evaluate specific neurochemical markers as a tool to monitor synaptic changes in future pre-clinical trials with HD models.

AUTHOR CONTRIBUTIONS

R.G.P. and G. O. obtained funding for this study and designed the experiments. N.Z., K.G., J.C., and D.Y. performed the experiments.

N.Z., K.G., J.C., and D.Y. prepared and analyzed the data. G.O. supervised the MRS data acquisition and analysis. R.G.P. supervised the ex vivo tissue collection and synapse analyses. L.E. supervised the statistical analyses. N.Z. and R.G.P. wrote the first draft of the manuscript and all authors edited subsequent versions and approved the final version of the manuscript.

ACKNOWLEDGMENTS

We thank Dr. Dinesh Deelchand for guidance in data analysis and assistance in LCModel basis set generation.

All experiments were conducted in compliance with the ARRIVE guidelines.

CONFLICT OF INTEREST

Dr. Öz consults for IXICO Technologies Limited and uniQure biopharma B.V., serves on the Scientific Advisory Board of BrainSpec Inc. and receives research support from Biogen.

DATA AVAILABILITY STATEMENT

The data that support the findings of this study are available from the corresponding author upon reasonable request. A preprint of this manuscript was previously published on BioRxiv. It can be found at https://doi.org/10.1101/2021.10.26.465951.

ORCID

Nicole Zarate https://orcid.org/0000-0003-4839-7783
Katherine Gundry https://orcid.org/0000-0002-3333-1709
Dahyun Yu https://orcid.org/0000-0002-3179-4080
Jordan Casby https://orcid.org/0000-0002-5601-3906
Lynn E. Eberly https://orcid.org/0000-0003-4763-330X
Gülin Öz https://orcid.org/0000-0002-5769-183X
Rocio Gomez-Pastor https://orcid.org/0000-0003-1136-5462

REFERENCES

Adanyeguh, I. M., Monin, M.-L., Rinaldi, D., Freeman, L., Durr, A., Lehéricy, S., Henry, P.-G., & Mochel, F. (2018). Expanded neurochemical profile in the early stage of Huntington disease using proton magnetic resonance spectroscopy. *NMR Biomed*, *31*. https://doi.org/10.1002/nbm.3880

Agarwal, S., Schaefer, M. L., Krall, C., & Johns, R. A. (2022). Isoflurane disrupts postsynaptic density-95 protein interactions causing neuronal synapse loss and cognitive impairment in juvenile mice *via* canonical NO-mediated protein Kinase-G signaling. *Anesthesiology*, *137*, 212–231.

Behrens, P. F., Franz, P., Woodman, B., Lindenberg, K. S., & Landwehrmeyer, G. B. (2002). Impaired glutamate transport and glutamate–glutamine cycling: downstream effects of the Huntington mutation. *Brain*, *125*, 1908–1922.

Cepeda, C., Wu, N., André, V. M., Cummings, D. M., & Levine, M. S. (2007). The corticostriatal pathway in Huntington's disease. *Progress in Neurobiology*, *81*, 253–271.

Deng, Y. P., Wong, T., Wan, J. Y., & Reiner, A. (2014). Differential loss of thalamostriatal and corticostriatal input to striatal projection neuron types prior to overt motor symptoms in the Q140 knock-in mouse model of Huntington's disease. *Frontiers in Systems Neuroscience*, *8*, 198.

Duarte, J. M. N., Do, K. Q., & Gruetter, R. (2014). Longitudinal neurochemical modifications in the aging mouse brain measured in vivo by 1H magnetic resonance spectroscopy. *Neurobiology of Aging*, *35*, 1660–1668.

Fan, M. M. Y., & Raymond, L. A. (2007). N-methyl-D-aspartate (NMDA) receptor function and excitotoxicity in Huntington's disease. *Progress in Neurobiology*, *81*, 272–293.

Finnema, S. J., Nabulsi, N. B., Eid, T., Detyniecki, K., Lin, S. F., Chen, M. K., Dhaher, R., Matuskey, D., Baum, E., Holden, D., Spencer, D. D., Mercier, J., Hannestad, J., Huang, Y., & Carson, R. E. (2016). Imaging synaptic density in the living human brain. *Science Translational Medicine*, *8*, 348ra96-348ra96.

Friedrich, J., Kordasiewicz, H. B., O'Callaghan, B., Handler, H. P., Wagener, C., Duvick, L., Swayze, E. E., Rainwater, O., Hofstra, B., Benneyworth, M., Nichols-Meade, T., Yang, P., Chen, Z., Ortiz, J. P., Clark, H. B., Öz, G., Larson, S., Zoghbi, H. Y., Henzler, C., & Orr, H. T. (2018). Antisense oligonucleotide–mediated ataxin-1 reduction prolongs survival in SCA1 mice and reveals disease-associated transcriptome profiles. *JCI Insight*, *3*, e123193.

Fujiyama, F., Kuramoto, E., Okamoto, K., Hioki, H., Furuta, T., Zhou, L., Nomura, S., & Kaneko, T. (2004). Presynaptic localization of an AMPA-type glutamate receptor in corticostriatal and thalamostriatal axon terminals. *European Journal of Neuroscience*, *20*, 3322–3330.

Garwood, M., & DelaBarre, L. (2001). The return of the frequency sweep: Designing adiabatic pulses for contemporary NMR. *Journal of Magnetic Resonance*, *153*, 155–177.

Gomez-Pastor, R., Burchfiel, E. T., Neef, D. W., Jaeger, A. M., Cabiscol, E., Mckinstry, S. U., Doss, A., Aballay, A., Lo, D. C., Akimov, S. S., Ross, C. A., Eroglu, C., & Thiele, D. J. (2017). Abnormal degradation of the neuronal stress-protective transcription factor HSF1 in Huntington's disease. *Nature Communications*, *8*, 14405.

Govindaraju, V., Young, K., & Maudsley, A. A. (2000). Proton NMR chemical shifts and coupling constants for brain metabolites. *NMR in Biomedicine*, *13*, 129–153.

Grachev, I. D., & Apkarian, A. V. (2001). Aging alters regional multichemical profile of the human brain: an in vivo1H-MRS study of young versus middle-aged subjects. *Journal of Neurochemistry*, *76*, 582–593.

Gruetter, R., & Tkác, I. (2000). Field mapping without reference scan using asymmetric echo-planar techniques. *Magnetic Resonance in Medicine*, *43*, 319–323.

Hassel, B., Tessler, S., Faull, R. L. M., & Emson, P. C. (2008). Glutamate uptake is reduced in prefrontal cortex in Huntington's disease. *Neurochemical Research*, *33*, 232–237.

Heikkinen, T., Lehtimäki, K., Vartiainen, N., Puoliväli, J., Hendricks, S. J., Glaser, J. R., Bradaia, A., Wadel, K., Touller, C., Kontkanen, O., Yrjänheikki, J. M., Buisson, B., Howland, D., Beaumont, V., Munoz-Sanjuan, I., & Park, L. C. (2012). Characterization of Neurophysiological and Behavioral Changes, MRI Brain Volumetry and 1H MRS in zQ175 Knock-In Mouse Model of Huntington's Disease. *PLoS One*, *7*, e50717.

Hennig, J., Nauerth, A., & Friedburg, H. (1986). RARE imaging: A fast imaging method for clinical MR. *Magnetic Resonance in Medicine*, *3*, 823–833.

Hsu, Y.-T., Chang, Y.-G., & Chern, Y. (2018). Insights into GABAAergic system alteration in Huntington's disease. *Royal Society Open Biology*, *8*, 180155.

Huerta-Ocampo, I., Mena-Segovia, J., & Bolam, J. P. (2014). Convergence of cortical and thalamic input to direct and indirect pathway medium spiny neurons in the striatum. *Brain Structure and Function*, *219*, 1787–1800.

Ippolito, D. M., & Eroglu, C. (2010). Quantifying synapses: An immunocytochemistry-based assay to quantify synapse number. *Journal of Visualized Experiments*, *45*, 1787–1800.

Joers, J. M., Deelchand, D. K., Lyu, T., Emir, U. E., Hutter, D., Gomez, C. M., Bushara, K. O., Eberly, L. E., & Öz, G. (2018). Neurochemical abnormalities in premanifest and early spinocerebellar ataxias. *Annals of Neurology*, *83*, 816–829.

Kolodziejczyk, K., & Raymond, L. A. (2016). Differential changes in thalamic and cortical excitatory synapses onto striatal spiny projection neurons in a Huntington disease mouse model. *Neurobiology of Disease*, *86*, 62–74.

Leavitt, B. R., Weir, D. W., & Sturrock, A. (2011). Development of biomarkers for Huntington's disease. *Lancet Neurology*, *10*, 573–590.

Li, D., Hérault, K., Silm, K., Evrard, A., Wojcik, S., Oheim, M., Herzog, E., & Ropert, N. (2013). Lack of evidence for vesicular glutamate transporter expression in mouse astrocytes. *The Journal of Neuroscience*, *33*, 4434–4455.

Lizarbe, B., Soares, A. F., Larsson, S., & Duarte, J. M. N. (2018). Neurochemical modifications in the hippocampus, cortex and hypothalamus of mice exposed to long-term high-fat diet. *Frontiers in Neuroscience*, *12*, 985.

Liévens, J. C., Woodman, B., Mahal, A., Spasic-Boscovic, O., Samuel, D., Kerkerian-Le, G. L., & Bates, G. P. (2001). Impaired glutamate uptake in the R6 Huntington's disease transgenic mice. *Neurobiology of Disease*, *8*, 807–821.

MacDonald, M. E., Ambrose, C. M., Duyao, M. P., Myers, R. H., Lin, C., Srinidhi, L., Barnes, G., Taylor, S. A., James, M., Groot, N., MacFarlane, H., Jenkins, B., Anderson, M. A., Wexler, N. S., Gusella, J. F., Bates, G. P., Basendale, S., Hummerich, H., Kirby, S., … Harper, P. S. (1993). A novel gene containing a trinucleotide repeat that is expanded and unstable on Huntington's disease chromosomes. *Cell*, *72*, 971–983.

Mckinstry, S. U., Karadeniz, Y. B., Worthington, A. K., Hayrapetyan, V. Y., Ozlu, M. I., Serafin-Molina, K., Risher, X. W. C., Ustunkaya, T., Dragatsis, I., Zeitlin, S., Yin, H. H., & Eroglu, C. (2014). Huntingtin is required for normal excitatory synapse development in cortical and striatal circuits. *Journal of Neuroscience*, *34*, 9455–9472.

Menalled, L. B., Kudwa, A. E., Miller, S., Fitzpatrick, J., Watson-Johnson, J., Keating, N., Ruiz, M., Mushlin, R., Alosio, W., McConnell, K., Connor, D., Murphy, C., Oakeshott, S., Kwan, M., Beltran, J., Ghavami, A., Brunner, D., Park, L. C., Ramboz, S., & Howland, D. (2012). Comprehensive behavioral and molecular characterization of a new knock-in mouse model of Huntington's disease: zQ175. *PLoS One*, *7*, e49838.

Murray, M. E., Przybelski, S. A., Lesnick, T. G., Liesinger, A. M., Spychalla, A., Zhang, B., Gunter, J. L., Parisi, J. E., Boeve, B. F., Knopman, D. S., Petersen, R. C., Jack, C. R., Jr., Dickson, D. W., & Kantarci, K. (2014). Early Alzheimer's disease neuropathology detected by proton MR spectroscopy. *Journal of Neuroscience*, *34*, 16247–16255.

Öz, G., Vollmers, M. L., Nelson, C. D., Shanley, R., Eberly, L. E., Orr, H. T., & Clark, H. B. (2011). In vivo monitoring of recovery from neurodegeneration in conditional transgenic SCA1 mice. *Experimental Neurology*, *232*, 290–298.

Öz, G., Nelson, C. D., Koski, D. M., Henry, P.-G., Marjanska, M., Deelchand, D. K., Shanley, R., Eberly, L. E., Orr, H. T., & Clark, H. B. (2010). Noninvasive detection of presymptomatic and progressive neurodegeneration in a mouse model of spinocerebellar ataxia type 1. *The Journal of Neuroscience*, *30*, 3831–3838.

Öz, G., Kittelson, E., Demirgoz, D., Rainwater, O., Eberly, L. E., Orr, H. T., & Clark, H. B. (2015). Assessing recovery from neurodegeneration in spinocerebellar ataxia 1: Comparison of in vivo magnetic resonance spectroscopy with motor testing, gene expression and histology. *Neurobiology of Disease*, *74*, 158–166.

Öz, G., Iltis, I., Hutter, D., Thomas, W., Bushara, K. O., & Gomez, C. M. (2011). Distinct neurochemical profiles of spinocerebellar ataxias 1, 2, 6, and cerebellar multiple system atrophy. *Cerebellum*, *10*, 208–217.

Öz, G. (Ed.). (2016). *Magnetic resonance spectroscopy of degenerative brain diseases*. Springer International Publishing.

Peng, Q., Wu, B., Jiang, M., Jin, J., Hou, Z., Zheng, J., Zhang, J., & Duan, W. (2016). Characterization of behavioral, neuropathological, brain metabolic and key molecular changes in zQ175 knock-in mouse model of Huntington's disease. *PLoS One*, *11*, e0148839.

Provencher, S. W. (1993). Estimation of metabolite concentrations from localized in vivo proton NMR spectra. *Magnetic Resonance in Medicine*, *30*, 672–679.

Ravalia, A. S., Lau, J., Barron, J. C., Purchase, S. L. M., Southwell, A. L., Hayden, M. R., Nafar, F., & Parsons, M. P. (2021). Super-resolution imaging reveals extrastriatal synaptic dysfunction in presymptomatic Huntington disease mice. *Neurobiology of Disease*, *152*, 105293. https://doi.org/10.1016/j.nbd.2021.105293

Raymond, L. A., André, V. M., Cepeda, C., Gladding, C. M., Milnerwood, A. J., & Levine, M. S. (2011). Pathophysiology of Huntington's disease: Time-dependent alterations in synaptic and receptor function. *Neuroscience*, *198*, 252–273.

Rebholz, H., Zhou, M., Nairn, A. C., Greengard, P., & Flajolet, M. (2013). Selective knockout of the casein kinase 2 in D1 medium spiny neurons controls dopaminergic function. *Biological Psychiatry*, *74*, 113–121.

Reiner, A., Albin, R. L., Anderson, K. D., D'Amato, C. J., Penney, J. B., & Young, A. B. (1988). Differential loss of striatal projection neurons in Huntington disease. *Proceedings of the National Academy of Sciences of the United States of America*, *85*, 5733–5737.

Skotte, N. H., Andersen, J. V., Santos, A., Aldana, B. I., Willert, C. W., Nørremølle, A., Waagepetersen, H. S., & Nielsen, M. L. (2018). Integrative characterization of the R6/2 mouse model of Huntington's disease reveals dysfunctional astrocyte metabolism. *Cell Reports*, *23*, 2211–2224.

Smith, Y., Raju, D., Nanda, B., Pare, J.-F., Galvan, A., & Wichmann, T. (2009). The Thalamostriatal systems: Anatomical and functional organization in normal and parkinsonian states. *Brain Research Bulletin*, *78*, 60–68.

Spokes, E. G. S., Garrett, N. J., Rossor, M. N., & Iversen, L. L. (1980). Distribution of GABA in post-mortem brain tissue from control, psychotic and Huntington's chorea subjects. *Journal of the Neurological Sciences*, *48*, 303–313.

Sturrock, A., Laule, C., Decolongon, J., Dar, S. R., Coleman, A. J., Creighton, S., Bechtel, N., Reilman, R., Hayden, M. R., Tabrizi, S. J., MacKay, A. L., & Leavitt, B. R. (2010). Magnetic resonance spectroscopy biomarkers in premanifest and early Huntington disease. *Neurology*, *75*, 1702–1710.

Sturrock, A., Laule, C., Wyper, K., Milner, R. A., Decolongon, J., Santos, R. D., Coleman, A. J., Carter, K., Creighton, S., Bechtel, N., Bohlen, S., Reilmann, R., Johnson, H. J., Hayden, M. R., Tabrizi, S. J., Mackay, A. L., & Leavitt, B. R. (2015). A longitudinal study of magnetic resonance spectroscopy Huntington's disease biomarkers. *Movement Disorders*, *30*, 393–401.

Sánchez-Pernaute, R., García-Segura, J. M., Barrio, A. A., Del, V. J., & De Yébenes, J. G. (1999). Clinical correlation of striatal 1H MRS changes in Huntington's disease. *Neurology*, *53*, 806–812.

Thomsen, M. B., Jacobsen, J., Lillethorup, T. P., Schacht, A. C., Simonsen, M., Romero-Ramos, M., Brooks, D. J., & Landau, A. M. (2021). In vivo imaging of synaptic SV2A protein density in healthy and striatal-lesioned rats with [11C]UCB-J PET. *Journal of Cerebral Blood Flow and Metabolism*, *41*, 819–830.

Tkác, I. (2008). Refinement of simulated basis set for LCModel analysis, in *16th Annual Meeting ISMRM*, p. 1624.

Tkác, I., Dubinsky, J. M., Keene, C. D., Gruetter, R., & Low, W. C. (2007). Neurochemical changes in Huntington R6/2 mouse striatum detected by in vivo1H NMR spectroscopy. *Journal of Neurochemistry*, *100*, 1397–1406.

Tkác, I., Starčuk, Z., Choi, I.-Y., & Gruetter, R. (1999). In Vivo 1 H NMR Spectroscopy of Rat Brain at 1 ms Echo Time. *Magnetic Resonance in Medicine*, *41*, 649–656.

Unschuld, P. G., Joel, S. E., Liu, X., Shanahan, M., Margolis, R. L., Biglan, K. M., Bassett, S. S., Schretlen, D. J., Redgrave, G. W., van Zijl,

P. C. M., Pekar, J. J., & Ross, C. A. (2012). Impaired cortico-striatal functional connectivity in prodromal Huntington's Disease. *Neuroscience Letters*, *514*, 204–209.

Yu, D., Zarate, N., White, A., Coates, D., Tsai, W., Nanclares, C., Cuccu, F., Yue, J. S., Brown, T. G., Mansky, R. H., Jiang, K., Kim, H., Nichols-Meade, T., Larson, S. N., Gundry, K., Zhang, Y., Tomas-Zapico, C., Lucas, J. J., Benneyworth, M., Öz, G., … Gomez-Pastor, R. (2022). CK2 alpha prime and alpha-synuclein pathogenic functional interaction mediates synaptic dysregulation in Huntington's disease. *Acta Neuropathologica Communications*, *10*, 83.

Zarate, N., Intihar, T. A., Yu, D., Sawyer, J., Tsai, W., Syed, M., Carlson, L., & Gomez-Pastor, R. (2021). Heat shock factor 1 directly regulates postsynaptic scaffolding PSD-95 in aging and huntington's disease and influences striatal synaptic density. *International Journal of Molecular Sciences*, *22*(23), 13113. https://doi.org/10.3390/ijms222313113

Zhang, C., Wu, Q., Liu, H., Cheng, L., Hou, Z., Mori, S., Hua, J., Ross, C. A., Zhang, J., Nopoulos, P. C., & Duan, W. (2020). Abnormal brain development in Huntington' Disease is recapitulated in the zQ175 knock-in mouse model. *Cerebral Cortex Communications*, *1*, 1–9.

Zhang, W., Gu, G.-J., Zhang, Q., Liu, J.-H., Zhang, B., Guo, Y., Wang, M.-Y., Gong, Q.-Y., & Xu, J.-R. (2017). NSCs promote hippocampal neurogenesis, metabolic changes and synaptogenesis in APP/PS1 transgenic mice. *Hippocampus*, *27*, 1250–1263.

SUPPORTING INFORMATION

Additional supporting information can be found online in the Supporting Information section at the end of this article.

How to cite this article: Zarate, N., Gundry, K., Yu, D., Casby, J., Eberly, L. E., Öz, G., & Gomez-Pastor, R. (2023). Neurochemical correlates of synapse density in a Huntington's disease mouse model. *Journal of Neurochemistry*, *164*, 226–241. https://doi.org/10.1111/jnc.15714